

Electronic Supplementary Information (ESI) for Nanoscale.
This journal is © The Royal Society of Chemistry 2018

Li⁺ Role in Upconversion Emission Enhancement of (YYbEr)₂O₃ Nanoparticles

Mengistie L. Debasu,^{a,b*} Jesse C. Riedl,^b J. Rocha,^b Luís D. Carlos^{a*}

^aDepartment of Physics and CICECO – Aveiro Institute of Materials, University of Aveiro, 3810-193 Aveiro, Portugal

^bDepartment of Chemistry and CICECO – Aveiro Institute of Materials, University of Aveiro, 3810-193 Aveiro, Portugal

*Corresponding author: *debasu@ua.pt; lcarlos@ua.pt*

Table of Contents

1. Review Table: Li ⁺ -induced Upconversion Enhancement	2
2. Quantum Yield Measurement Setup	6
3. Crystallite Size and Rietveld Refinement	6
4. Electron Microscopy	9
5. Infrared Spectroscopy	10
6. Thermogravimetry	10
7. Radiant and Luminous Fluxes	11
8. References	13

1. Review Table: Li⁺-induced Upconversion Enhancement

Table S1. Enhancement factors and proposed enhancement mechanisms for Li⁺-doped materials excited at 980 nm with laser diodes. The optimal concentration of Li that gives the highest upconversion emission intensity/quantum yield was considered. The enhancement factor is the ratio of the integrated emission intensity of a given Ln³⁺ transition with and without Li⁺. Except for this work (quantum yield measurements), in the other listed examples the enhancement is qualitatively quantified by the comparison of upconversion intensities.

Materials	Synthesis Method	Enhancement Factor	Enhancement Mechanisms
(Y _{0.939} Yb _{0.02} Er _{0.01} Li _{0.031}) ₂ O ₃ ^{This work}	Solid-state	10 (Er ³⁺ visible emission)	Lattice parameter shrinkage and increase in crystallite size; reduced number of quenching centers (e.g., OH ⁻ and CO ₃ ²⁻ groups) can be ruled out.
NaLuF ₄ :4%Yb/0.1%Tm/7%Li ¹	Co-precipitation	18 (Tm ³⁺ ¹ G ₄ → ³ H ₆ emission at 480 nm) 7 (Tm ³⁺ ³ H ₄ → ³ H ₆ emission at 804 nm)	
NaLuF ₄ :20%Yb/1%Tm/20%Er/15%Li ²	Hydrothermal	13.7 (Er ³⁺ ⁴ F _{9/2} → ⁴ I _{15/2} emission at 660 nm)	
NaYF ₄ :5%Yb/1%Er/30%Li ³	Hydrothermal	7 (Er ³⁺ ² H _{11/2} , ⁴ S _{3/2} → ⁴ I _{15/2} emissions) 5 (Er ³⁺ ⁴ F _{9/2} → ⁴ I _{15/2} emission)	
NaYF ₄ :18%Yb/2%Er/4%Li ⁴	Hydrothermal	2 (Er ³⁺ ² H _{11/2} , ⁴ S _{3/2} → ⁴ I _{15/2} emission at 540 nm) 3.3 (Er ³⁺ ⁴ F _{9/2} → ⁴ I _{15/2} emission at 652 nm)	
NaYF ₄ :20%Yb/1%Tm/15%Li ⁵	Hydrothermal	10 (Tm ³⁺ ¹ G ₄ → ³ H ₆ emission at 477 nm) 9 (Tm ³⁺ ¹ G ₄ → ³ F ₄ emission at 649 nm)	
NaYF ₄ :20%Yb/1%Ho/15%Li ⁵	Hydrothermal	12 (Ho ³⁺ ⁵ F ₄ , ⁵ S ₂ → ⁵ I ₈ emission at 538 nm) 3 (Ho ³⁺ ⁵ F ₅ → ⁵ I ₈ emission at 644 nm)	
NaGdF ₄ : 20%Yb/1%Tm/4%Li@NaGdF ₄ ⁶ NaGdF ₄ : 20%Yb/2%Er/4%Li@NaGdF ₄ ⁶ NaGdF ₄ : 20%Yb/2%Ho/4%Li@NaGdF ₄ ⁶	Co-precipitation	428 (Tm ³⁺ ¹ G ₄ → ³ H ₆ emission at 474 nm) 46 (Er ³⁺ ² H _{11/2} , ⁴ S _{3/2} → ⁴ I _{15/2} emission at 545 nm) 37 (Ho ³⁺ ⁵ F ₄ , ⁵ S ₂ → ⁵ I ₈ emission at 540 nm)	
Gd ₂ O ₃ :1%Er/10%Li ⁷	Co-precipitation	3.3 (Er ³⁺ ² H _{11/2} , ⁴ S _{3/2} → ⁴ I _{15/2} emission at 545 nm)	
Gd ₂ O ₃ :2%Yb/0.5%Ho/4%Li ⁸	Solid-state	10 (Ho ³⁺ ⁵ F ₄ , ⁵ S ₂ → ⁵ I ₈ emission at 550 nm) 4 (Ho ³⁺ ⁵ F ₅ → ⁵ I ₈ emission at 660 nm)	
Gd ₂ O ₃ :0.75%Er/3%Li ⁹	Co-precipitation	9.76 (Er ³⁺ ² H _{11/2} , ⁴ S _{3/2} → ⁴ I _{15/2} emission at 561 nm) 6.24 (Er ³⁺ ⁴ F _{9/2} → ⁴ I _{15/2} emission at 660 nm)	
Y ₂ O ₃ :2%Er/3%Li ¹⁰	Solid-state	12.5 (Er ³⁺ ² H _{11/2} , ⁴ S _{3/2} → ⁴ I _{15/2} emission at 560 nm) 7.5 (Er ³⁺ ⁴ F _{9/2} → ⁴ I _{15/2} emission at 660 nm)	
TiO ₂ :10%Yb/1%Er/20%Li ¹¹	Solid-state	800 (Er ³⁺ ² H _{11/2} , ⁴ S _{3/2} → ⁴ I _{15/2} emission at 550 nm) 350 (Er ³⁺ ⁴ F _{9/2} → ⁴ I _{15/2} emission at 660 nm)	

TiO ₂ :10%Yb/1%Er/20%Li ¹²	Solid-state	130 (Er^{3+} $^2\text{H}_{11/2}, ^4\text{S}_{3/2} \rightarrow ^4\text{I}_{15/2}$ emission at 550 nm) 21 (Er^{3+} $^4\text{F}_{9/2} \rightarrow ^4\text{I}_{15/2}$ emission at 660 nm)
ZnO:2%Er/3%Li ¹³	Solid-state	14 (Er^{3+} $^2\text{H}_{11/2}, ^4\text{S}_{3/2} \rightarrow ^4\text{I}_{15/2}$ emission at 557 nm)
Zn ₂ SiO ₄ :3%Yb/0.5%Er/1%Li ¹⁴	Microwave sintering	6 (Er^{3+} $^2\text{H}_{11/2}, ^4\text{S}_{3/2} \rightarrow ^4\text{I}_{15/2}$ emission at 550 nm)
ZrO ₂ :12%Yb/0.5%Er/0.5%Li ¹⁵	Solid-state	1.93 (Er^{3+} $^2\text{H}_{11/2}, ^4\text{S}_{3/2} \rightarrow ^4\text{I}_{15/2}$ emission at 550 nm) 1.65 (Er^{3+} $^4\text{F}_{9/2} \rightarrow ^4\text{I}_{15/2}$ emission at 660 nm)
CaMoO ₄ :8%Yb/0.5%Tm/5%Li ¹⁶	Solid-state	10 (Tm^{3+} $^1\text{G}_4 \rightarrow ^3\text{H}_6$ emission at 476 nm) 4 (Tm^{3+} $^3\text{F}_2 \rightarrow ^3\text{H}_6$ emission at 647 nm) 10 (Tm^{3+} $^3\text{H}_4 \rightarrow ^3\text{H}_6$ emission at 800 nm)
CaMoO ₄ :8%Yb/2%Er/10%Li ¹⁷	Solid-state	6 (Er^{3+} $^2\text{H}_{11/2}, ^4\text{S}_{3/2} \rightarrow ^4\text{I}_{15/2}$ emission at 550 nm)
CaWO ₄ :10%Yb/5%Er/15%Li ¹⁸ CaMoO ₄ :10%Yb/5%Er/15%Li ¹⁸ SrWO ₄ :10%Yb/5%Er/15%Li ¹⁸ SrMoO ₄ :10%Yb/5%Er/15%Li ¹⁸	Solid-state	2, 3, 3 and 2 (Er^{3+} $^2\text{H}_{11/2}, ^4\text{S}_{3/2} \rightarrow ^4\text{I}_{15/2}$ emission at 550 nm)
YMoO ₄ :4%Yb/0.5%Ho/2%Li ¹⁹	Co-precipitation	104 (Ho^{3+} $^5\text{F}_4, ^5\text{S}_2 \rightarrow ^5\text{I}_8$ emission at 549 nm) 160 (Ho^{3+} $^5\text{F}_5 \rightarrow ^5\text{I}_8$ emission at 650 nm)
Gd ₆ MoO ₁₂ :8%Yb/0.16%Er/35%Li ²⁰	Solid-state	5 (Er^{3+} $^2\text{H}_{11/2}, ^4\text{S}_{3/2} \rightarrow ^4\text{I}_{15/2}$ emission at 550 nm) 8 (Er^{3+} $^4\text{F}_{9/2} \rightarrow ^4\text{I}_{15/2}$ emission at 660 nm)
Gd ₆ MoO ₁₂ :10%Yb/0.2%Er/0.5%Tm/15%Li ²¹	Solid-state	1.1 (Tm^{3+} $^1\text{G}_4 \rightarrow ^3\text{H}_6$ emission at 475 nm) 2 (Er^{3+} $^2\text{H}_{11/2}, ^4\text{S}_{3/2} \rightarrow ^4\text{I}_{15/2}$ emission at 550 nm) 2 (Er^{3+} $^4\text{F}_{9/2} \rightarrow ^4\text{I}_{15/2}$ emission at 660 nm)
NaZnPO ₄ :1%Yb/0.3%Er/1%Li ²²	Solid-state	2.5 (Er^{3+} $^2\text{H}_{11/2}, ^4\text{S}_{3/2} \rightarrow ^4\text{I}_{15/2}$ emission at 550 nm) 2 (Er^{3+} $^4\text{F}_{9/2} \rightarrow ^4\text{I}_{15/2}$ emission at 660 nm)
CaSnO ₃ :8%Yb/1%Er/10%Li ²³	Solid-state	1.5 (Er^{3+} $^4\text{F}_{9/2} \rightarrow ^4\text{I}_{15/2}$ emission at 675 nm)
NaYF ₄ :20%Yb/0.5%Tm/7%Li ²⁴	Co-precipitation	8 (Tm^{3+} $^1\text{D}_2 \rightarrow ^3\text{F}_4$ emission at 452 nm) 5 (Tm^{3+} $^1\text{G}_4 \rightarrow ^3\text{H}_6$ emission at 479 nm)
Y ₂ Ti ₂ O ₇ :7.5%Yb/1%Er/10%Li ²⁵	Solid-state	8.3 (Er^{3+} $^2\text{H}_{11/2}, ^4\text{S}_{3/2} \rightarrow ^4\text{I}_{15/2}$ emission at 550 nm) 18.6 (Er^{3+} $^4\text{F}_{9/2} \rightarrow ^4\text{I}_{15/2}$ emission at 660 nm)
Gd ₂ O ₃ :3%Yb/0.5%Tm/6%Li ²⁶	Reverse microemulsion	10 (Tm^{3+} $^1\text{G}_4 \rightarrow ^3\text{H}_6$ emission at 476 nm)
Gd ₂ O ₃ :2%Yb/0.3%Ho/20%Li ²⁷	Co-precipitation and Solid-state	3.5 (Ho^{3+} $^5\text{F}_4, ^5\text{S}_2 \rightarrow ^5\text{I}_8$ emission 549 nm)
Y ₂ O ₃ :4%Yb/1%Ho/3%Li ²⁸	Solid-state	10 (Ho^{3+} $^5\text{F}_4, ^5\text{S}_2 \rightarrow ^5\text{I}_8$ emission 550 nm) 4 (Ho^{3+} $^5\text{F}_5 \rightarrow ^5\text{I}_8$ emission at 660 nm)
Y ₂ O ₃ :5%Yb/1%Ho/5%Li ²⁹	Solid-state	8 (Ho^{3+} $^5\text{F}_4, ^5\text{S}_2 \rightarrow ^5\text{I}_8$ emission at 549 nm)
Y ₂ O ₃ :3%Yb/0.1%Tb/2%Li ³⁰	Solid-state	2 (Tb^{3+} $^5\text{D}_4 \rightarrow ^7\text{F}_5$ emission at 547 nm)
Y ₂ O ₃ : 3.5%Yb/0.5%Er/0.3%Tm/2%Li ³¹	Solid-state	3.5 (Tm^{3+} $^1\text{G}_4 \rightarrow ^3\text{H}_6$ emission at 480 nm) 2.9 (Er^{3+} $^2\text{H}_{11/2}, ^4\text{S}_{3/2} \rightarrow ^4\text{I}_{15/2}$ emission at 560 nm) 2.5 (Er^{3+} $^4\text{F}_{9/2} \rightarrow ^4\text{I}_{15/2}$ emission at 660 nm)

Distortion of local crystal field symmetry and improvement of the crystallinity

Distortion of local crystal field symmetry and decrease of quenching centers (e.g., OH⁻, CO₃²⁻ and NO_x groups)

ZrO ₂ :12%Yb/0.5%Er/0.5%Li ³²	Solid-state	1.65 ($\text{Er}^{3+} \text{ }^4\text{F}_{9/2} \rightarrow \text{ }^4\text{I}_{15/2}$ emission at 660 nm)	
Y ₃ Al ₅ O ₁₂ :1%Er/7%Li ³³	Solid-state	4.6 ($\text{Er}^{3+} \text{ }^2\text{H}_{11/2}, \text{ }^4\text{S}_{3/2} \rightarrow \text{ }^4\text{I}_{15/2}$ emission at 550 nm) 3.5 ($\text{Er}^{3+} \text{ }^4\text{F}_{9/2} \rightarrow \text{ }^4\text{I}_{15/2}$ emission at 660 nm)	
Y ₂ O ₃ :3%Yb/0.3%Er/5%Li ³⁴	Solid-state	2 ($\text{Er}^{3+} \text{ }^2\text{H}_{11/2}, \text{ }^4\text{S}_{3/2} \rightarrow \text{ }^4\text{I}_{15/2}$ emission at 560 nm) 4 ($\text{Er}^{3+} \text{ }^4\text{F}_{9/2} \rightarrow \text{ }^4\text{I}_{15/2}$ emission at 660 nm)	
Lu ₂ O ₃ :2%Yb/0.5%Tm/7%Li ³⁵	Solid-state	4 ($\text{Tm}^{3+} \text{ }^1\text{G}_4 \rightarrow \text{ }^3\text{H}_6$ emission at 490 nm) 3 ($\text{Tm}^{3+} \text{ }^1\text{G}_4 \rightarrow \text{ }^3\text{F}_4$ emission at 653 nm)	Distortion of local crystal field symmetry, increase in particle size and reduction of quenching centers (e.g., OH and NO _x groups)
Gd ₂ O ₃ :10%Yb/2%Er/1.5%Zn/4%Li ³⁶	Co-precipitation	4 ($\text{Er}^{3+} \text{ }^2\text{H}_{11/2}, \text{ }^4\text{S}_{3/2} \rightarrow \text{ }^4\text{I}_{15/2}$ emission at 561 nm) 10 ($\text{Er}^{3+} \text{ }^4\text{F}_{9/2} \rightarrow \text{ }^4\text{I}_{15/2}$ emission at 660 nm)	
CaWO ₄ :5%Yb/5%Er/10%Li ³⁷	Solid-state	1.4 ($\text{Er}^{3+} \text{ }^2\text{H}_{11/2}, \text{ }^4\text{S}_{3/2} \rightarrow \text{ }^4\text{I}_{15/2}$ emission at 550 nm) 1.7 ($\text{Er}^{3+} \text{ }^4\text{F}_{9/2} \rightarrow \text{ }^4\text{I}_{15/2}$ emission at 660 nm)	Distortion of local crystal field symmetry and charge compensation
SiO ₂ -Al ₂ O ₃ -ZnF ₂ -SrF ₂ :1%Er/1.5%Li ³⁸	Melting and quenching	5 ($\text{Er}^{3+} \text{ }^2\text{H}_{11/2}, \text{ }^4\text{S}_{3/2} \rightarrow \text{ }^4\text{I}_{15/2}$ emission at 550 nm) 12 ($\text{Er}^{3+} \text{ }^4\text{F}_{9/2} \rightarrow \text{ }^4\text{I}_{15/2}$ emission at 660 nm)	
NaYF ₄ :18%Yb/2%Er/80%Li ³⁹	Hydrothermal	3 ($\text{Er}^{3+} \text{ }^2\text{H}_{11/2}, \text{ }^4\text{S}_{3/2} \rightarrow \text{ }^4\text{I}_{15/2}$ emission at 545 nm)	Distortion of local crystal field symmetry and phase transition
NaGdF ₄ :20%Yb/2%Er/7%Li ⁴⁰	Co-precipitation	47 ($\text{Er}^{3+} \text{ }^2\text{H}_{11/2}, \text{ }^4\text{S}_{3/2} \rightarrow \text{ }^4\text{I}_{15/2}$ emissions) 23 ($\text{Er}^{3+} \text{ }^4\text{F}_{9/2} \rightarrow \text{ }^4\text{I}_{15/2}$ emission)	Distortion of local crystal field symmetry and decrease in the activator ions' inter-ionic interaction
NaYF ₄ :20%Yb/2%Tm/20%Li ⁴¹	Co-precipitation	3 ($\text{Tm}^{3+} \text{ }^1\text{G}_4 \rightarrow \text{ }^3\text{H}_6$ emission at 480 nm) 3 ($\text{Tm}^{3+} \text{ }^3\text{F}_{2,3} \rightarrow \text{ }^3\text{H}_6$ emission at 700 nm) 2 ($\text{Tm}^{3+} \text{ }^3\text{H}_4 \rightarrow \text{ }^3\text{H}_6$ emission at 800 nm)	Modification of interstitial sites and increased crystallite size
Y ₂ O ₃ :2%Er/5%Li ⁴²	Solid-state	80 ($\text{Er}^{3+} \text{ }^2\text{H}_{11/2}, \text{ }^4\text{S}_{3/2} \rightarrow \text{ }^4\text{I}_{15/2}$ emission at 560 nm)	Increase in Er ³⁺ ground state absorption
Y ₂ O ₃ :1%Er/5%Li ⁴³	Solid-state	60 ($\text{Er}^{3+} \text{ }^4\text{G}_{11/2}, \text{ }^2\text{H}_{9/2} \rightarrow \text{ }^4\text{I}_{15/2}$ emission at 402 nm) 45 ($\text{Er}^{3+} \text{ }^2\text{H}_{11/2}, \text{ }^4\text{S}_{3/2} \rightarrow \text{ }^4\text{I}_{15/2}$ emission at 560 nm)	Increased lifetime in the Er ³⁺ excited state of the $^4\text{S}_{3/2}$ and $^4\text{I}_{11/2}$ levels
Y ₂ O ₃ :0.2%Er/5%Li ⁴⁴ Y ₂ O ₃ :0.2%Er/2.5%Zn/5%Li ⁴⁴	Solid-state	11 and 28 ($\text{Er}^{3+} \text{ }^2\text{H}_{11/2}, \text{ }^4\text{S}_{3/2} \rightarrow \text{ }^4\text{I}_{15/2}$ emission at 560 nm)	Distortion of local crystal field symmetry, reduction of the OH groups, and prolonged lifetime of the Er ³⁺ $^4\text{I}_{11/2}$ level
Y ₂ O ₃ :2%Yb/1%Er/5%Li ⁴⁵	Solid-state	33 ($\text{Er}^{3+} \text{ }^4\text{G}_{11/2}, \text{ }^4\text{H}_{9/2} \rightarrow \text{ }^4\text{I}_{15/2}$ emissions at 390 and 409 nm) 24 ($\text{Er}^{3+} \text{ }^2\text{H}_{11/2}, \text{ }^4\text{S}_{3/2} \rightarrow \text{ }^4\text{I}_{15/2}$ emission at 564 nm)	Distortion of local crystal field symmetry, and prolonged excited-state lifetimes of Er ³⁺ $^4\text{S}_{3/2}$ and Yb ³⁺ $^2\text{F}_{3/2}$ levels
Y ₂ O ₃ :7%Yb/4%Er/0.5%Li ⁴⁶	Solid-state	4 ($\text{Er}^{3+} \text{ }^2\text{H}_{11/2}, \text{ }^4\text{S}_{3/2} \rightarrow \text{ }^4\text{I}_{15/2}$ emission at 563 nm) 8 ($\text{Er}^{3+} \text{ }^4\text{F}_{9/2} \rightarrow \text{ }^4\text{I}_{15/2}$ emission at 660 nm)	Distortion of local crystal field symmetry and charge transfer from localized states
Y ₂ O ₃ :2%Yb/1%Er/5%Li ⁴⁷	Solid-state	25.0 ($\text{Er}^{3+} \text{ }^2\text{H}_{11/2}, \text{ }^4\text{S}_{3/2} \rightarrow \text{ }^4\text{I}_{15/2}$ emission at 563 nm) 8.1 ($\text{Er}^{3+} \text{ }^4\text{F}_{9/2} \rightarrow \text{ }^4\text{I}_{15/2}$ emission at 660 nm)	Distortion of local crystal field symmetry, prolonged excited-state lifetimes of the Er ³⁺ $^4\text{I}_{11/2}$ and Yb ³⁺ $^2\text{F}_{5/2}$ levels, and dispersion of clusters of activator ions
Y ₂ O ₃ :1%Er/5%Li ⁴⁸	Solid-state	11.5 (Er ³⁺ red to green emission intensity ratio)	Distortion of local crystal field symmetry, prolonged excited-state lifetimes of the Er ³⁺ $^4\text{I}_{11/2}$ level and enlarged nanocrystal size
Y ₂ O ₃ :5%Yb/0.25%Tm/5%Li ⁴⁹	Solid-state	14 ($\text{Tm}^{3+} \text{ }^3\text{H}_4 \rightarrow \text{ }^3\text{H}_6$ emission at 811 nm)	Distortion of local crystal field symmetry, dispersion of clusters of activator ions, and creation of oxygen vacancies

$\text{Y}_2\text{O}_3:14\%\text{Er}/4\%\text{Li}^{50}$	Ultrasonic spray pyrolysis	365 ($\text{Er}^{3+} \text{H}_{11/2}, \text{S}_{3/2} \rightarrow \text{I}_{15/2}$ emission at 550 nm) 171 ($\text{Er}^{3+} \text{F}_{9/2} \rightarrow \text{I}_{15/2}$ emission at 675 nm)	Distortion of the crystal field symmetry, creation of localized states, increase in the population of ${}^4\text{F}_{7/2}$ state and the reduction of the non-radiative decays.
$\text{Lu}_6\text{O}_5\text{F}_8:20\%\text{Yb}/1\%\text{Er}/3\%\text{Li}^{51}$	Co-precipitation	5 ($\text{Er}^{3+} \text{H}_{11/2}, \text{S}_{3/2} \rightarrow \text{I}_{15/2}$ emission at 550 nm) 13 ($\text{Er}^{3+} \text{F}_{9/2} \rightarrow \text{I}_{15/2}$ emission at 675 nm)	Distortion of local crystal field symmetry, reduced number of OH^- and carbonate groups, and enlarged nanocrystal size
$\text{CeO}_2:1\%\text{Er}/10\%\text{Li}^{52}$	Solid-state	3 ($\text{Er}^{3+} \text{H}_{11/2}, \text{S}_{3/2} \rightarrow \text{I}_{15/2}$ emission at 550 nm) 8 ($\text{Er}^{3+} \text{F}_{9/2} \rightarrow \text{I}_{15/2}$ emission at 675 nm)	Distortion of local crystal field symmetry, improved crystallinity, creation of oxygen vacancies and reduction of quenching centers
$\text{BaTiO}_3:2\%\text{Er}/3\%\text{Li}^{53}$	Solid-state	56 ($\text{Er}^{3+} \text{H}_{11/2}, \text{S}_{3/2} \rightarrow \text{I}_{15/2}$ emission at 550 nm) 52 ($\text{Er}^{3+} \text{F}_{9/2} \rightarrow \text{I}_{15/2}$ emission at 675 nm)	Distortion of local crystal field symmetry, creation of oxygen vacancies and reduction of the OH groups
$\text{BaTiO}_3:5\%\text{Yb}/1\%\text{Er}/7\%\text{Li}^{54}$	Solid-state	22 ($\text{Er}^{3+} \text{H}_{11/2}, \text{S}_{3/2} \rightarrow \text{I}_{15/2}$ emission at 550 nm) 11 ($\text{Er}^{3+} \text{F}_{9/2} \rightarrow \text{I}_{15/2}$ emission at 660 nm)	Distortion of local crystal field symmetry and longer lifetime of the $\text{Er}^{3+} \text{S}_{3/2}$ and $\text{F}_{9/2}$ levels
$\text{Bi}_2\text{Ti}_2\text{O}_7:3\%\text{Yb}/3\%\text{Er}/1.5\%\text{Li}^{55}$	Template assisted	14 ($\text{Er}^{3+} \text{H}_{11/2}, \text{S}_{3/2} \rightarrow \text{I}_{15/2}$ emission at 550 nm) 20 ($\text{Er}^{3+} \text{F}_{9/2} \rightarrow \text{I}_{15/2}$ emission at 660 nm)	Distortion of local crystal field symmetry and reduction of surface defects
$\text{TiO}_2:0.1\%\text{Er}/2\%\text{Li}^{56}$	Solid-state	18 ($\text{Er}^{3+} \text{H}_{11/2}, \text{S}_{3/2} \rightarrow \text{I}_{15/2}$ emission at 550 nm) 8 ($\text{Er}^{3+} \text{F}_{9/2} \rightarrow \text{I}_{15/2}$ emission at 663 nm)	Distortion of local crystal field symmetry and increased Er-O bond length
$\text{Y}_3\text{Al}_5\text{O}_{12}:1\%\text{Er}/13\%\text{Li}^{57}$	Solid-state	36 ($\text{Er}^{3+} \text{H}_{11/2}, \text{S}_{3/2} \rightarrow \text{I}_{15/2}$ emission at 560 nm) 23 ($\text{Er}^{3+} \text{F}_{9/2} \rightarrow \text{I}_{15/2}$ emission at 660 nm)	Distortion of local crystal field symmetry and prolonged lifetime of $\text{Er}^{3+} \text{I}_{11/2}$ level
$\text{Y}_2\text{SiO}_5:1.2\%\text{Pr}/10\%\text{Li}^{58}$	Solid-state	9 ($\text{Pr}^{3+} \text{4f5d} \rightarrow \text{3H}_4$ emission at 276 nm)	Reduction in clustering of the Pr^{3+} ions, flux effect/crystallite size enlargement and phase change
$\text{GdVO}_4:20\%\text{Yb}/1\%\text{Ho}/10\%\text{Li}^{59}$	Solid-state	2.2 ($\text{Ho}^{3+} \text{5F}_4, \text{5S}_2 \rightarrow \text{5I}_8, \text{5F}_5 \rightarrow \text{5I}_8$ and $\text{5F}_4, \text{5S}_2 \rightarrow \text{5I}_7$ emissions)	Distortion of local crystal field symmetry, dispersion of activator ions pairings and creation of oxygen vacancies
$\text{GdVO}_4:20\%\text{Yb}/1.5\%\text{Er}/5\%\text{Li}^{60}$	Solid-state	4 ($\text{Er}^{3+} \text{H}_{11/2}, \text{S}_{3/2} \rightarrow \text{I}_{15/2}$ emission at 550 nm)	Crystallite size enlargement, small number of activator ions on the surface, breakage of activator ions pairing
$\text{GdVO}_4:22\%\text{Yb}/1.8\%\text{Ho}/1\%\text{Tm}/8\%\text{Li}^{61}$	Solid-state	6.0 ($\text{Tm}^{3+} \text{1G}_4 \rightarrow \text{3H}_6$ emission at 480 nm) 4.5 ($\text{Ho}^{3+} \text{5F}_4, \text{5S}_2 \rightarrow \text{5I}_8$ emission at 550 nm) 4.2 ($\text{Tm}^{3+} \text{3H}_4 \rightarrow \text{3H}_6$ emission at 805 nm)	Occupation of interstitial sites and decrease in Ln^{3+} interatomic distance

2. Quantum Yield Measurement Setup

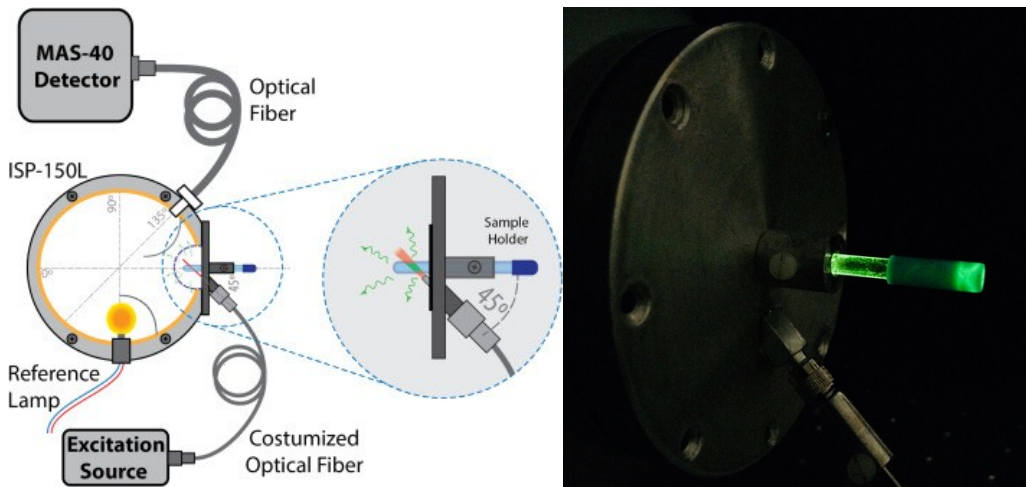


Figure S1. Scheme of the experimental setup used to measure the emission quantum yields.^{62,63} The sample holder is illuminated using a customized optical fiber that guides the excitation radiation. The emission is collected by the ISP-150L integrating sphere and then guided through an optical fiber to the CCD of the MAS-40 detector, that quantifies the radiant spectral flux $S(\lambda)$. Photo showing the partial view of the integrated sphere window, the customized optical fiber guiding the 980-nm laser to the sample illumination area of the quartz tube sample holder; the green color along the wall of the quartz tube is due to the reflection of the Er^{3+} visible upconversion emission from the illuminated sample volume under the 980 nm laser excitation.

3. Crystallite Size and Rietveld Refinement

The average crystallite sizes of the nanoparticles was calculated using Scherrer's equation:

$$D = \frac{K\lambda}{\beta \cos \theta} \quad (\text{S1})$$

where, D is the average size of the crystal, K is the Scherrer's shape factor constant (0.94), λ is the wavelength of the X-rays (1.5406 Å) and β is the full-width at half maximum (FWHM), in radians, of the diffraction peak at 2θ . The instrumental line broadening factor (0.063°) at $2\theta=29.15^\circ$ was subtracted from β . The error in the crystallite size is estimated by:

$$\delta D = D \sqrt{\left(\frac{\delta \beta}{\beta}\right)^2 + (\tan \theta \delta \theta)^2} \quad (\text{S2})$$

where $\delta \beta$ (between 0.001 and 0.002 rad) is the error in the FWHM determined from the Gaussian fitting and $\delta \theta$ (0.0065°) is the resolution in θ .

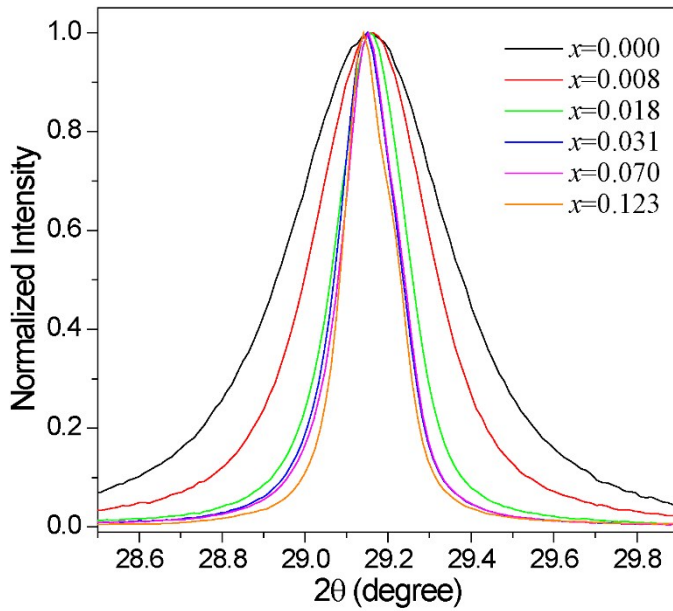


Figure S2. Dependence of the FWHM of a given XRD peak on the Li^+ content.

Figure S3 shows the Rietveld refinement of the diffraction patterns of the nanoparticles. Refinement parameters R_p , R_{wp} , R_{exp} and Chi Squared are: (0.00728, 0.00943, 0.00481, 1.9605), (0.008225, 0.01187, 0.00479, 2.4806), (0.01067, 0.01491, 0.00476, 3.132), (0.01160, 0.01711, 0.00476, 3.5914) and (0.01128, 0.01741, 0.00479, 3.6317) for $x=0.000$, 0.008, 0.018, 0.031 and 0.070, respectively.

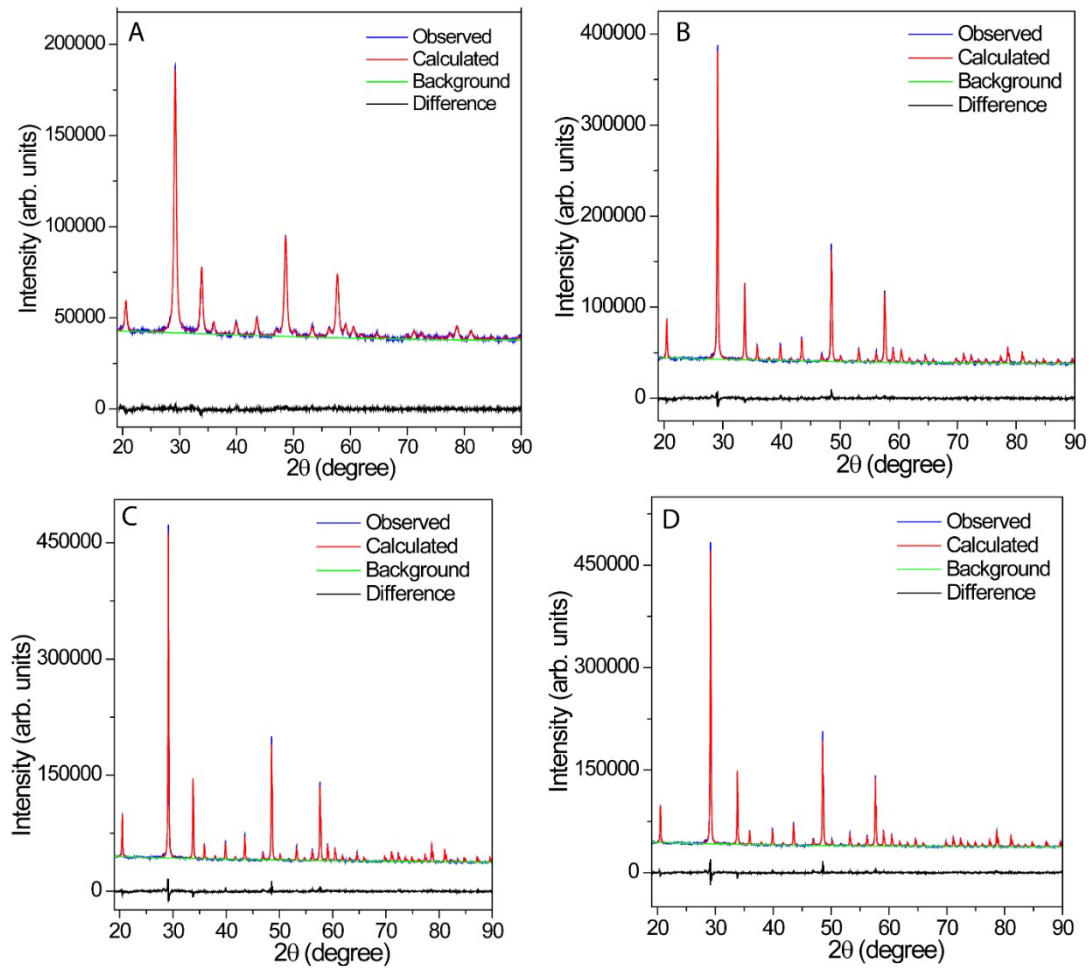


Figure S3. Rietveld refinement of powder XRD patterns of $(Y_{0.97-x}Yb_{0.02}Er_{0.01}Li_x)_2O_3$ nanoparticles: A) $x=0.000$, B) $x=0.018$, C) $x=0.031$ and D) $x=0.070$.

4. Electron Microscopy

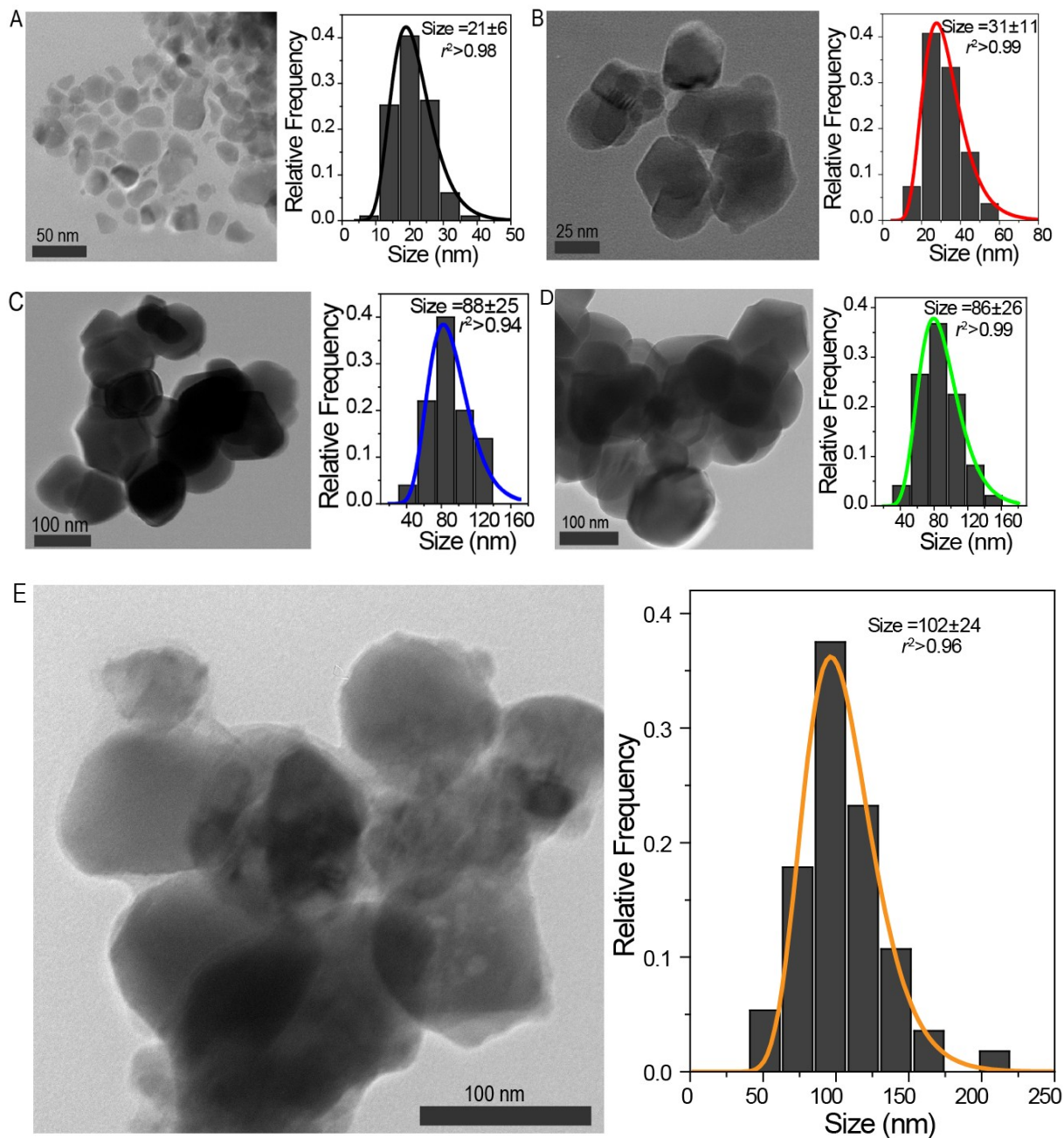


Figure S4. Representative TEM images of the nanoparticles A) $x=0.000$, B) $x=0.008$, C) $x=0.018$, D) $x=0.031$ and E) $x=0.123$. The corresponding particle size distribution histograms are shown on the right of each image (solid lines of the histogram are the best fits using a log-normal distribution).

5. Infrared Spectroscopy

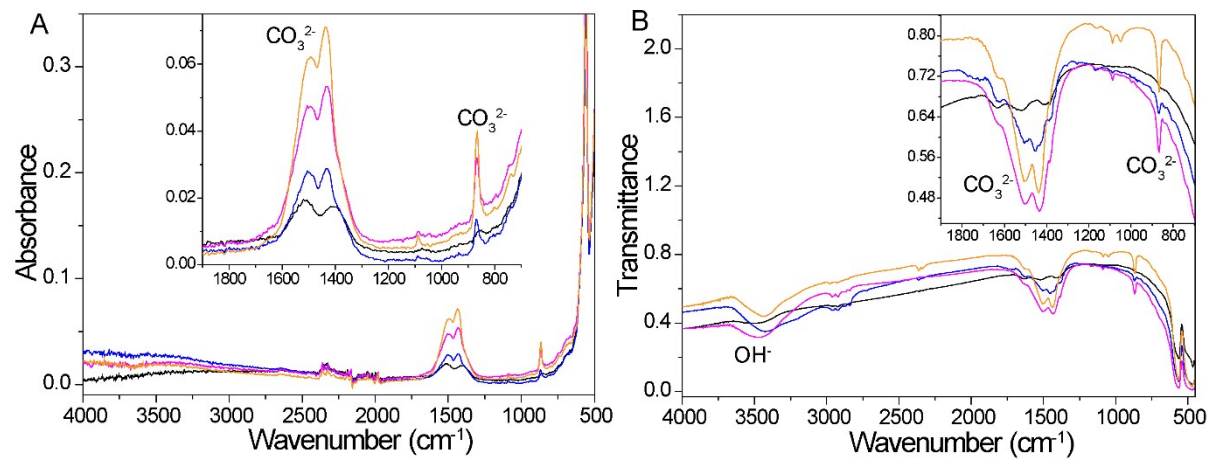


Figure S5. FTIR spectra of the nanoparticles, A) absorbance, B) transmittance: $x=0.000$ (black lines) $x=0.031$ (blue), $x=0.070$ (magenta) and $x=0.123$ (orange). The insets in A) and B) show the carbonate bands in the range of 700 to 1900 cm^{-1} .

6. Thermogravimetry

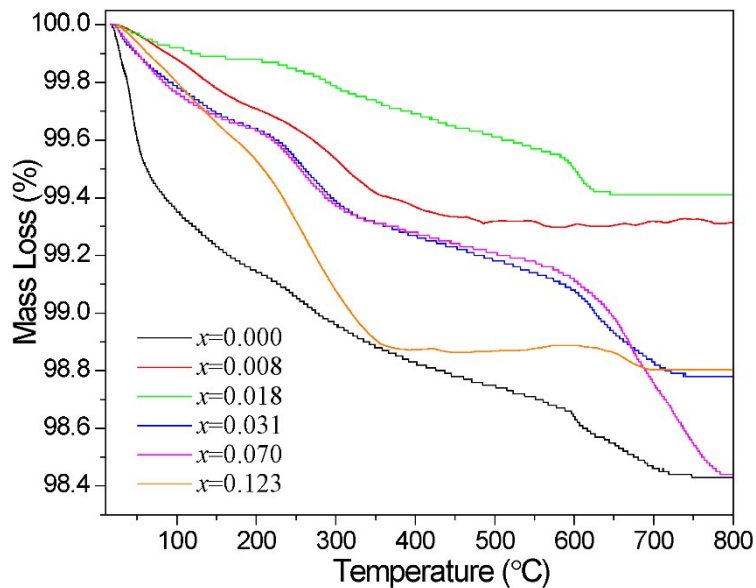


Figure S6. TG curves of the nanoparticles.

7. Radiant and Luminous Fluxes

The radiant flux R (in W) was computed from the measured spectral radiant flux $S(\lambda)$ measured with the integrated sphere:

$$R = \int_{\lambda_{\min}}^{\lambda_{\max}} S(\lambda) d\lambda \quad (\text{S3})$$

The luminous flux L (lm) was calculated from the measured spectral radiant flux and the tabulated relative photopic luminous efficacy function $V(\lambda)$,⁶⁴ at the maximum luminescence efficacy value (683 lm·W⁻¹):⁶⁵

$$L \equiv 683 \cdot \int_{\lambda_{\min}}^{\lambda_{\max}} S(\lambda) V(\lambda) d\lambda \quad (\text{S4})$$

The radiant and luminous flux values computed from Equation S3 and S4 are summarized in Table S2.

Table S2. Radiant and luminous flux values of the nanoparticles upon 980 nm laser excitation.

Laser power	x=0.000		x=0.008		x=0.018		x=0.031		x=0.070	
density (W cm ⁻²)	Radiant flux (×10 ⁻⁶ W)	Luminous flux (×10 ⁻³ lm)	Radiant flux (×10 ⁻⁶ W)	Luminous flux (×10 ⁻³ lm)	Radiant flux (×10 ⁻⁶ W)	Luminous flux (×10 ⁻³ lm)	Radiant flux (×10 ⁻⁶ W)	Luminous flux (×10 ⁻³ lm)	Radiant flux (×10 ⁻⁶ W)	Luminous flux (×10 ⁻³ lm)
14.63	0.57	0.07	1.11	0.22	4.34	1.07	5.63	1.28	6.09	1.42
37.01	2.02	0.31	2.46	0.50	11.45	2.94	15.48	3.67	16.06	3.95
59.38	3.35	0.50	6.37	1.36	25.37	6.77	32.86	8.17	27.72	7.12
81.76	6.68	1.08	10.68	2.38	47.33	13.05	56.43	14.39	51.41	13.77
104.14	9.18	1.54	15.26	3.55	75.21	21.32	83.48	21.73	71.40	19.51
126.52	12.05	2.10	19.66	4.67	93.96	27.20	110.78	29.29	89.69	25.06
148.90	14.78	2.66	24.03	5.85	117.73	34.73	134.02	36.27	106.91	30.30
171.27	17.44	3.22	27.77	6.88	136.44	40.39	155.39	42.55	125.13	36.08
193.65	20.98	4.02	34.36	8.67	172.00	52.14	197.21	54.61	146.68	42.50
238.41	29.61	6.05	50.45	13.30	243.19	78.01	286.96	81.28	201.86	60.58
283.16	36.45	7.83	65.72	17.77	291.24	95.41	357.71	104.55	242.68	74.35
327.92	42.40	9.47	75.44	20.91	333.93	111.26	464.38	138.81	280.25	86.94
372.68	47.15	10.84	83.56	23.50	363.21	122.62	426.87	133.69	300.11	94.51
417.43	54.78	13.09	97.24	28.12	426.54	146.35	483.52	155.84	341.61	110.03
462.19	65.09	16.17	117.92	34.84	487.79	170.67	544.01	178.39	383.42	125.37
506.94	65.32	16.73	137.85	40.29	527.29	186.68	578.51	192.59	427.56	141.53
551.70	75.21	19.83	136.93	41.41	537.57	191.78	597.08	201.07	441.04	147.64
641.21	83.67	23.14	149.68	46.57	607.06	219.80	656.98	225.58	473.18	161.31

8. References

- 1 M. Hu, D. D. Ma, Y. Z. Cheng, C. C. Liu, Z. P. Zhang, Y. J. Cai, S. Wu and R. F. Wang, *J. Mater. Chem. B*, 2017, **5**, 2662–2670.
- 2 H. Lin, D. Xu, A. Li, D. Teng, S. Yang and Y. Zhang, *Sci. Rep.*, 2016, **6**, 28051.
- 3 A. Dubey, A. K. Soni, A. Kumari, R. Dey and V. K. Rai, *J. Alloys Compd.*, 2017, **693**, 194–200.
- 4 Y. L. Ding, X. D. Zhang, H. B. Gao, S. Z. Xu, C. C. Wei and Y. Zhao, *J. Alloys Compd.*, 2014, **599**, 60–64.
- 5 H. Lin, D. K. Xu, D. D. Teng, S. H. Yang and Y. L. Zhang, *Opt. Mater. (Amst.)*, 2015, **45**, 229–234.
- 6 M. Ding, Y. Ni, Y. Song, X. Liu, T. Cui, D. Chen, Z. Ji, F. Xu, C. Lu and Z. Xu, *J. Alloys Compd.*, 2015, **623**, 42–48.
- 7 H. H. T. Vu, T. S. Atabaev, N. D. Nguyen, Y. H. Hwang and H. K. Kim, *J. Sol-Gel Sci. Technol.*, 2014, **71**, 391–395.
- 8 Y. T. Jia, Y. L. Song, Y. F. Bai and Y. X. Wang, *Luminescence*, 2011, **26**, 259–263.
- 9 A. P. Jadhav, J. H. Oh, S. W. Park, H. Choi, B. K. Moon, B. C. Choi, K. Jang, J. H. Jeong, S. S. Yi and J. H. Kim, *Curr. Appl. Phys.*, 2016, **16**, 1374–1381.
- 10 Y. Bai, K. Yang, Y. Wang, X. Zhang and Y. Song, *Opt. Commun.*, 2008, **281**, 2930–2932.
- 11 B. S. Cao, Y. Y. He, Y. Sun, M. Song and B. Dong, *J. Nanosci. Nanotechnol.*, 2011, **11**, 9899–9903.
- 12 B. S. Cao, Y. Y. He, Z. Q. Feng, M. Song and B. Dong, *Opt. Commun.*, 2011, **284**, 3311–3314.
- 13 H. L. Han, L. W. Yang, Y. X. Liu, Y. Y. Zhang and Q. B. Yang, *Opt. Mater. (Amst.)*, 2008, **31**, 338–341.
- 14 L. Jiang, S. Xiao, X. Yang, J. Ding and K. Dong, *Appl. Phys. B-Lasers Opt.*, 2012, **107**, 477–481.
- 15 L. Liu, Y. X. Wang, X. R. Zhang, K. Yang, Y. F. Bai, C. H. Huang, W. L. Han, C. L. Li and Y. L. Song, *Opt. Mater. (Amst.)*, 2011, **33**, 1234–1238.
- 16 J. H. Chung, S. Y. Lee, K. B. Shim, S. Y. Kweon, S. C. Ur and J. H. Ryu, *Appl. Phys. a-Materials Sci. Process.*, 2012, **108**, 369–373.
- 17 J. H. Chung, J. H. Ryu, J. W. Eun, J. H. Lee, S. Y. Lee, T. H. Heo and K. B. Shim, *Mater. Chem. Phys.*, 2012, **134**, 695–699.
- 18 J. H. Kim, H. Choi, E. O. Kim, H. M. Noh, B. K. Moon and J. H. Jeong, *Opt. Mater. (Amst.)*, 2014, **38**, 113–118.
- 19 M. Mondal, V. K. Rai, C. Srivastava, S. Sarkar and R. Akash, *J. Appl. Phys.*, 2016, **120**, 233101.
- 20 J. Y. Sun, B. Xue and H. Y. Du, *Infrared Phys. Technol.*, 2013, **60**, 10–14.
- 21 J. Y. Sun, B. Xue and H. Y. Du, *Opt. Commun.*, 2013, **298**, 37–40.
- 22 L. Mukhopadhyay, V. K. Rai, R. Bokolia and K. Sreenivas, *J. Lumin.*, 2017, **187**, 368–377.
- 23 T. Pang, W. H. Lu and W. J. Shen, *Phys. B-Condensed Matter*, 2016, **502**, 11–15.
- 24 C. Zhao, X. Kong, X. Liu, L. Tu, F. Wu, Y. Zhang, K. Liu, Q. Zeng and H. Zhang, *Nanoscale*, 2013, **5**, 8084–8089.
- 25 Z. S. Chen, T. F. Chen, W. P. Gong, W. Y. Xu, D. Y. Wang and Q. K. Wang, *J. Am. Ceram. Soc.*, 2013, **96**, 1857–1862.
- 26 Q. Sun, H. Zhao, X. Q. Chen, F. P. Wang, W. Cai and Z. H. Jiang, *Mater. Chem. Phys.*, 2010, **123**, 806–810.

- 27 P. Singh, P. K. Shahi, A. Rai, A. Bahadur and S. B. Rai, *Opt. Mater. (Amst.)*, 2016, **58**, 432–438.
- 28 Y. F. Bai, Y. X. Wang, G. Y. Peng, K. Yang, X. R. Zhang and Y. L. Song, *J. Alloys Compd.*, 2009, **478**, 676–678.
- 29 R. V. Yadav, S. K. Singh and S. B. Rai, *Rsc Adv.*, 2015, **5**, 26321–26327.
- 30 A. Pandey, V. K. Rai and K. Kumar, *Spectrochim. Acta Part a-Molecular Biomol. Spectrosc.*, 2014, **118**, 619–623.
- 31 Y. F. Bai, Y. X. Wang, G. Y. Peng, W. Zhang, Y. K. Wang, K. Yang, X. R. Zhang and Y. L. Song, *Opt. Commun.*, 2009, **282**, 1922–1924.
- 32 L. Liu, Y. X. Wang, X. R. Zhang, K. Yang, Y. F. Bai, C. H. Huang and Y. L. Song, *Opt. Commun.*, 2011, **284**, 1876–1879.
- 33 M. Z. Yang, Y. Sui, H. W. Mu, S. C. Lu, X. J. Wang and T. Q. Lu, *J. Rare Earths*, 2011, **29**, 1022–1025.
- 34 K. Mishra, S. K. Singh, A. K. Singh and S. B. Rai, *Mater. Res. Bull.*, 2013, **48**, 4307–4313.
- 35 L. Li, X. T. Wei, X. Q. Cao, K. M. Deng, Q. H. Chen, Y. H. Chen, C. X. Guo and M. Yin, *J. Nanosci. Nanotechnol.*, 2011, **11**, 9892–9898.
- 36 D. G. Li, W. P. Qin, P. Zhang, L. L. Wang, M. Lan and P. B. Shi, *Opt. Mater. Express*, 2017, **7**, 329–340.
- 37 D. H. Kim, J. H. Ryu, J. H. Chung, K. B. Shim and S. Y. Cho, *J. Electrochem. Soc.*, 2011, **158**, J345–J348.
- 38 W. Y. He, X. F. Wang, J. Zheng and X. H. Yan, *Mater. Res. Innov.*, 2014, **18**, 376–379.
- 39 Q. Q. Dou and Y. Zhang, *Langmuir*, 2011, **27**, 13236–13241.
- 40 Q. Cheng, J. H. Sui and W. Cai, *Nanoscale*, 2012, **4**, 779–784.
- 41 M. Misiak, B. Cichy, A. Bednarkiewicz and W. Strek, *J. Lumin.*, 2014, **145**, 956–962.
- 42 T. Fan and J. Lu, *Opt. Commun.*, 2013, **300**, 5–7.
- 43 G. Y. Chen, H. C. Liu, H. J. Liang, G. Somesfalean and Z. G. Zhang, *Solid State Commun.*, 2008, **148**, 96–100.
- 44 H. J. Liang, Y. D. Zheng, G. Y. Chen, L. Wu, Z. G. Zhang and W. W. Cao, *J. Alloys Compd.*, 2011, **509**, 409–413.
- 45 H. J. Liang, G. Y. Chen, H. C. Liu and Z. G. Zhang, *J. Lumin.*, 2009, **129**, 197–202.
- 46 E. F. Huerta, S. Carmona-Tellez, S. Gallardo-Hernandez, J. G. Cabanas-Moreno and C. Falcony, *Ecs J. Solid State Sci. Technol.*, 2016, **5**, R129–R135.
- 47 G. Y. Chen, H. C. Liu, H. J. Liang, G. Somesfalean and Z. G. Zhang, *J. Phys. Chem. C*, 2008, **112**, 12030–12036.
- 48 G. Y. Chen, H. C. Liu, G. Somesfalean, Y. Q. Sheng, H. J. Liang, Z. G. Zhang, Q. Sun and F. P. Wang, *Appl. Phys. Lett.*, 2008, **92**, 113114.
- 49 D. Y. Li, Y. X. Wang, X. R. Zhang, H. X. Dong, L. Liu, G. Shi and Y. L. Song, *J. Appl. Phys.*, 2012, **112**, 094701.
- 50 A. N. Meza-Rocha, E. F. Huerta, U. Caldiño, S. Carmona-Téllez, M. Bettinelli, A. Speghini, S. Pelli, G. C. Righini and C. Falcony, *J. Lumin.*, 2015, **167**, 352–359.
- 51 L. N. Guo, Y. H. Wang, Y. Z. Wang, J. Zhang, P. Y. Dong and W. Zeng, *Nanoscale*, 2013, **5**, 2491–2504.
- 52 Y. Y. Guo, D. Y. Wang and F. Wang, *Opt. Mater. (Amst.)*, 2015, **42**, 390–393.
- 53 Q. Sun, X. Q. Chen, Z. K. Liu, F. P. Wang, Z. H. Jiang and C. Wang, *J. Alloys Compd.*, 2011, **509**, 5336–5340.
- 54 X. Q. Chen, Z. K. Liu, Q. Sun, M. Ye and F. P. Wang, *Opt. Commun.*, 2011, **284**, 2046–2049.
- 55 Y. K. Cun, Z. W. Yang, J. Y. Liao, J. B. Qiu, Z. G. Song and Y. Yang, *Mater. Lett.*,

- 2014, **131**, 154–157.
- 56 B. S. Cao, Z. Q. Feng, Y. Y. He, H. Li and B. Dong, *J. Sol-Gel Sci. Technol.*, 2010, **54**, 101–104.
- 57 M. Z. Yang, Y. Sui, S. P. Wang, X. J. Wang, Y. Q. Sheng, Z. G. Zhang, T. Q. Lu and W. F. Liu, *Chem. Phys. Lett.*, 2010, **492**, 40–43.
- 58 E. L. Cates, A. P. Wilkinson and J. H. Kim, *J. Phys. Chem. C*, 2012, **116**, 12772–12778.
- 59 T. V Gavrilovic, D. J. Jovanovic, L. V Trandafilovic and M. D. Dramicanin, *Opt. Mater. (Amst.)*, 2015, **45**, 76–81.
- 60 T. V Gavrilovic, D. J. Jovanovic, V. M. Lojpur, V. Dordevic and M. D. Dramicanin, *J. Solid State Chem.*, 2014, **217**, 92–98.
- 61 V. Mahalingam, R. Naccache, F. Vetrone and J. A. Capobianco, *Opt. Express*, 2012, **20**, 111–119.
- 62 S. Balabhadra, M. L. Debasu, C. D. S. Brites, R. A. S. Ferreira and L. D. Carlos, *J. Lumin.*, 2017, **189**, 64–70.
- 63 C. D. S. Brites, X. Xie, M. L. Debasu, X. Qin, R. Chen, W. Huang, J. Rocha, X. Liu and L. D. Carlos, *Nat. Nanotechnol.*, 2016, **11**, 851–856.
- 64 S. J. Williamson and H. Z. Cummins, *Light and Color in Nature and Art*, Wiley, New York, 1983.
- 65 A. Ryer, *Light Measurement Handbook*, International Light Inc, Newburyport, Massachusetts, 1997.